

All-polarization-maintaining tunable L-band mode-locked fiber laser and cascaded second-harmonic generation

Kang-Rui Chang(常康瑞), Xiang Zhang(张祥), Cheng-Jie Gao(高承杰), Hao-Bin Zheng(郑浩斌), Yong Shen(沈咏), and Hong-Xin Zou(邹宏新)

Citation: Chin. Phys. B, 2026, 35 (**8**): 084209. DOI: 10.1088/1674-1056/ae3133
http://cpb.iphy.ac.cn; http://iopscience.iop.org/cpb

What follows is a list of articles you may be interested in

Generation of wavelength-tunable, bound-state and noise-like pulses in an all-polarization-maintaining laser ring cavity based on nonlinear polarization evolution

Yazhou Shi(石亚洲), Ze Li(李泽), and Zhiguo Lv(吕志国)
Chin. Phys. B, 2026, 35 (**5**): 054202. DOI: 10.1088/1674-1056/ae15f3

Generation of spectrally uncorrelated biphotons via fiber nonlinear quantum interference

Zhengtong Wei(卫正统), Chuan Qu(瞿川), Tian'an Wu(吴天安), Yuanyuan Li(李媛媛), Bo Li(李博), and Shenghai Zhang(张胜海)
Chin. Phys. B, 2023, 32 (**6**): 064202. DOI: 10.1088/1674-1056/acb767

Wavelength and sensitivity tunable long period gratings fabricated in fluid-cladding microfibers

Wa Jin(金娃), Linke Zhang(张林克), Xiang Zhang(张祥), Ming Xu(徐铭), Weihong Bi(毕卫红), and Yuefeng Qi(齐跃峰)
Chin. Phys. B, 2022, 31 (**1**): 014207. DOI: 10.1088/1674-1056/ac3394

Square microcavity semiconductor lasers

Yuede Yang(杨跃德), Haizhong Weng(翁海中), Youzeng Hao(郝友增), Jinlong Xiao(肖金龙), Yongzhen Huang(黄永箴)
Chin. Phys. B, 2018, 27 (**11**): 114212. DOI: 10.1088/1674-1056/27/11/114212

Tunable wavelength filters using polymer long-period waveguide gratings based on metal-cladding directly defined technique

Ji-Hou Wang(王继厚), Chang-Ming Chen(陈长鸣), Yang Zheng(郑洋), Xi-Bin Wang(王希斌), Yun-Ji Yi(衣云骥), Xiao-Qiang Sun(孙小强), Fei Wang(王菲), Da-Ming Zhang(张大明)
Chin. Phys. B, 2017, 26 (**2**): 024212. DOI: 10.1088/1674-1056/26/2/024212

All-polarization-maintaining tunable L-band mode-locked fiber laser and cascaded second-harmonic generation

Kang-Rui Chang(常康瑞)[1,2], Xiang Zhang(张祥)[1,2,3], Cheng-Jie Gao(高承杰)[1,2], Hao-Bin Zheng(郑浩斌)[1,2], Yong Shen(沈咏)[1,2,†], and Hong-Xin Zou(邹宏新)[1,2,3,‡]

[1] *Institute for Quantum Science and Technology, College of Science, National University of Defense Technology, Changsha* 410073, *China*
[2] *Hunan Key Laboratory of Mechanism and Technology of Quantum Information, Changsha* 410073, *China*
[3] *National Key Laboratory for Positioning, Navigation and Timing Technology, Changsha* 410073, *China*

(Received 20 October 2025; revised manuscript received 23 December 2025; accepted manuscript online 26 December 2025)

There is an urgent demand for highly stable, broadly wavelength-tunable, and low-repetition-rate pulsed lasers in fields such as cold-atom physics, precision spectroscopy, and bioimaging. However, conventional L-band lasers often suffer from environmental instability and limited tuning range. To address this, we propose an all-polarization-maintaining, wavelength-tunable L-band mode-locked fiber laser, followed by cascaded second harmonic generation. Wavelength tuning from 1570 nm to 1596 nm was achieved by incorporating a rotatable intracavity filter with a bandwidth of 10 nm. The laser exhibits self-starting mode locking and can generate pulses with a pulse width of 87 ps and a repetition rate of 15.6 MHz. Using cascaded periodically poled lithium niobate and β-barium borate crystals, we perform frequency conversion on the output pulses to produce tunable near-infrared (778–804 nm) and ultraviolet (389–402 nm) light. With broad wavelength tunability enabling applications such as two-photon excitation fluorescence imaging at 780 nm, laser cooling of calcium ions at 397 nm, and optical pumping in miniaturized rubidium atomic clocks, this laser system can serve as a versatile platform for quantum technologies and ultrafast spectroscopy.

Keywords: tunable wavelength, all-polarization-maintaining, harmonic generation, ultraviolet light source

PACS: 42.25.Ja, 42.81.Gs, 42.55.Wd, 42.60.Gd

DOI: 10.1088/1674-1056/ae3133 **CSTR:** 32038.14.CPB.ae3133

1. Introduction

Owing to their ability to operate in the long-wavelength range (1565–1625 nm), L-band laser sources offer distinct advantages. Specifically, in optical communications, the L-band provides a crucial extension to the C-band (1530–1565 nm), thereby expanding the available wavelength range of fiber-optic transmission systems and alleviating congestion in the C-band.[1] In biomedical applications, L-band lasers exhibit deeper tissue penetration than shorter-wavelength near-infrared sources due to reduced scattering and absorption in biological tissue, which significantly improves the signal-to-noise ratio and image quality in optical coherence tomography.[2–4] In quantum precision science, the 780–800 nm visible light that can be generated from the L-band via second-harmonic generation (SHG) serves as an excitation source for two-photon fluorescence[5] and for magneto-optical trapping of rubidium atoms.[6] Further frequency doubling of the 790-nm light produces ultraviolet (UV) light at 397 nm, which can be used for the laser cooling of calcium ions, $^{40}Ca^{+}$, via ground-to-excited-state transitions.[7] Although ideal as fundamental sources for these critical wavelengths, existing L-band fiber lasers primarily employ non-polarization-maintaining (non-PM) or multimode fibers, resulting in output polarization states that are environmentally unstable. This instability severely restricts their use in precision scientific instruments requiring long-term stability.

Various approaches to L-band fiber laser generation have been reported.[8–12] Although erbium-doped fiber (EDF) is widely used as a gain medium, its gain spectrum exhibits a peak in the C-band. Studies show that the effective gain window of EDF can be shifted toward the L-band by adjusting the cavity loss, fiber length, and doping concentration.[13,14] Experimental results demonstrate that optimizing the EDF length and pump power can suppress C-band lasing, thereby enabling stable and tunable L-band operation.[15,16] The integration of established wavelength-tuning techniques, including mechanical stretching of fiber gratings, polarization control, 45° tilted grating switching, and thermo-optic mechanical tuning,[17–27] enables broadband wavelength selection and rapid switching in L-band lasers.

The nonlinear amplifying ring mirror (NALM) is a key technology for generating ultrashort pulses owing to its high stability and ease of implementation.[28–32] However, existing research has primarily focused on the C-band wavelength range,[33–36] while systematic exploration of all-PM NALM systems operating in the L-band remains limited. Although

†Corresponding author. E-mail: shenyong08@nudt.edu.cn
‡Corresponding author. E-mail: hxzou@nudt.edu.cn

© 2026 Chinese Physical Society and IOP Publishing Ltd. All rights, including for text and data mining, AI training, and similar technologies, are reserved.

significant progress has been made in harmonic generation using nonlinear crystals,[37–41] most systems are designed for fixed wavelengths. Consequently, they are poorly suited to the dynamic wavelength-matching needs of tunable L-band lasers. Moreover, research into efficient fourth-harmonic generation (FHG) of wavelengths in the UV spectral region remains limited.

This paper proposes an all-PM mode-locked tunable L-band fiber laser based on an NALM. The system employs a cascaded SHG scheme to effectively address challenges in stability and wavelength tuning. Wavelength tuning is enabled by a rotating optical bandpass filter (BPF) inside the cavity. Meanwhile, a cascaded SHG setup, comprising periodically poled lithium niobate (PPLN) and β-barium borate (BBO) crystals, produces both second-harmonic (778–804 nm) and fourth-harmonic (389–400 nm) outputs. The 397 nm fourth-harmonic pulses, with durations on the order of hundreds of picoseconds, can serve as a probe source for time-resolved studies of quantum state dynamics during ion cooling processes. This temporal scale is orders of magnitude better than the millisecond frame rates of conventional CCD-based imaging systems. At a pump power of 320 mW in the L-band fiber laser, the system achieves a second-harmonic (near-infrared) conversion efficiency of 21% and a fourth-harmonic (ultraviolet) efficiency of 2.4%. Its compact, all-fiber design provides a versatile platform for trapped-ion quantum experiments and ultrafast optics, offering wavelength flexibility, high temporal resolution, and environmental robustness.

2. Experimental setup and working principle

Figure 1 shows the system from pulse generation to UV output. The setup includes a tunable L-band mode-locked fiber laser serving as the seed laser, a dual-stage erbium-doped fiber amplifier (EDFA) for power scaling, and a cascaded SHG unit for frequency conversion. The seed laser employs a polarizing beam splitter collimator (semi-PBS) to form a figure-of-nine cavity configuration. The fiber loop comprises a wavelength division multiplexer (WDM), a 64 cm gain fiber (Er80-4/125-HD-PM, Liekki), a semi-PBS, and a 10 m passive PM fiber (PM-1550-XP). In the free-space segment, a Faraday rotator (FR), a BPF centered at 1590 nm with a 12 nm bandwidth (FBH1590-12, Thorlabs), a quarter-wave plate (QWP), and a PBS are arranged in sequence to enable mode locking through the interference of the two counterpropagating beams in the cavity. The total cavity length is 11.72 m. The group velocity dispersion (GVD) of the passive PM fiber at 1550 nm is -22.8 ps^2/km, whereas the EDF has a GVD of 28.04 ps^2/km.

The seed laser is coupled into the dual-stage EDFA via a fiber collimator (Col1). The preamplifier stage employs forward and backward pumping by 976 nm semiconductor lasers with maximum output powers of 610 mW and 1000 mW, respectively. Its 62 cm-long gain fiber (Er80-4/125-HD-PM, Liekki) is placed between WDM1 and WDM2. Both pumps for the main amplifier stage have a maximum power of 1 W, and its gain fiber (Er80-4/125-HD-PM, Liekki) has a length of 188 cm. The amplified light is then coupled to the cascaded SHG unit by a fiber collimator (Col2). The unit consists of a PPLN crystal (MSHG1550-0.5-1, Covesion), a BBO crystal (NLC02, Thorlabs), a half-wave plate (HWP), a dichroic mirror (DM), and four lenses.

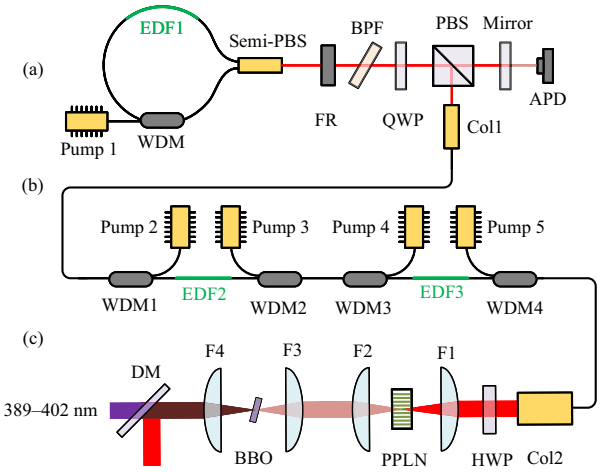


Fig. 1. (a) Experimental setup of the tunable L-band mode-locked fiber laser. (b) Dual-stage erbium-doped fiber amplifier (EDFA). (c) Cascaded SHG setup. BPF, band pass filter; Semi-PBS, PBS collimator; Col, fiber collimator; FR, Faraday rotator; QWP, quarter-wave plate; HWP, half-wave plate; DM, dichroic mirror; WDM, wavelength division multiplexer.

In our experiment, wavelength tuning was achieved by rotating the angle of the filter. When incident light enters the filter, it undergoes multiple reflections and transmissions between the highly reflective coatings on both sides, forming multiple-beam interference. Only when the optical path difference of the light wave traveling back and forth in the cavity meets the condition for constructive interference can light of a specific wavelength be transmitted efficiently. Based on the principle of multibeam interference, the relationship model between the central wavelength of transmitted light and the angle of incidence for a narrowband interference filter under oblique incidence is described by the following equation:

$$\lambda = \lambda_0 \sqrt{1 - \left(\frac{n \sin\theta}{N}\right)^2}, \tag{1}$$

where λ_0 is the central wavelength of the incident light, N is the effective refractive index of the filter, n is the refractive index of air, θ is the angle of incidence, and λ is the central wavelength of the transmitted light.[42,43]

We inserted the rotatable narrowband filter (FBH1590-12, Thorlabs) into the cavity. The simulation results in Fig. 2(a) show that the central transmission wavelength can be continuously tuned from 1560 nm to 1590 nm as the filter tilt

angle varies over a 20° range. The experimental measurements shown in Fig. 2(b) confirm this tuning range; over the same 20° tilt range, the central transmission wavelength blueshifts. Figure 2(c) illustrates the relationship between the central wavelength and the rotation angle. Both theoretical and experimental results show a blueshift trend, with the target wavelength of 1588 nm lying within the tunable range. In the experiment, the relationship between the rotation angle and the central wavelength is approximately linear, rather than exhibiting a rapid decline with increasing rotation angle. This is because the EDF provides lower gain at longer wavelengths, which slows down the shift of the central wavelength as the rotation angle increases.

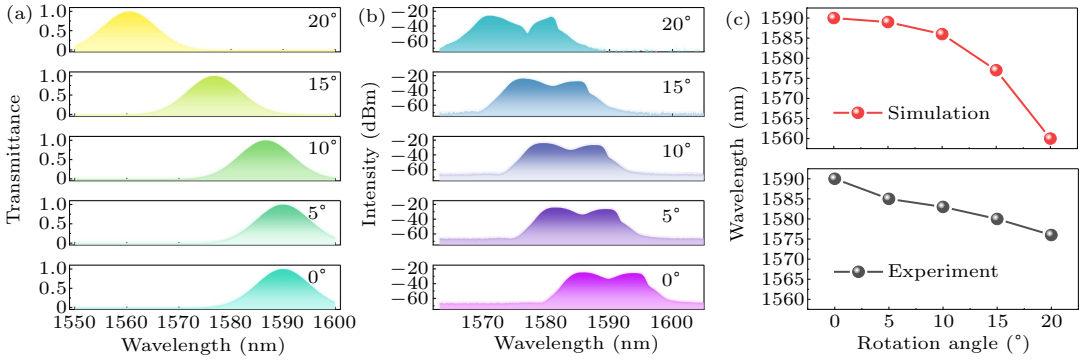


Fig. 2. (a) Calculated transmittance spectra of the filter at different angles. (b) Measured output spectra of the fiber laser at different filter angles. (c) Comparison of the calculated and experimental central wavelengths as a function of the filter angle.

3. Results and discussion

To investigate the influence of the pump power on the spectral characteristics of the seed laser, the optical spectra were measured using an optical spectrum analyzer (MS9710C, Anritsu), as shown in Fig. 3. Substantial changes were observed in both the Kelly sidebands and the central spectral structure as the pump power increased. At the relatively low pump power of 200–320 mW, the intracavity nonlinearity remained at a low level, resulting in a smooth spectral envelope. When the pump power was increased to 340–420 mW, the mode-locked laser operated in a metastable state, leading to pronounced spike structures within the spectral envelope. As the pump power was raised further to 440–480 mW, a renewed balance between nonlinearity, dispersion, loss, and gain was achieved, allowing the laser to enter a new steady state and producing a smooth spectral envelope once again. Finally, at 500–600 mW, the laser returned to a metastable state with heightened nonlinearity, resulting in more intricate spectral spikes within the spectral envelope. Notably, across the entire adjusted power range, the shift in the central wavelength of the spectrum was less than 5 nm. This indicates that effective wavelength tuning cannot be achieved by simply varying the pump power, and nonlinear effects exert a much stronger influence on the spectral envelope than on the shift of the central wavelength.

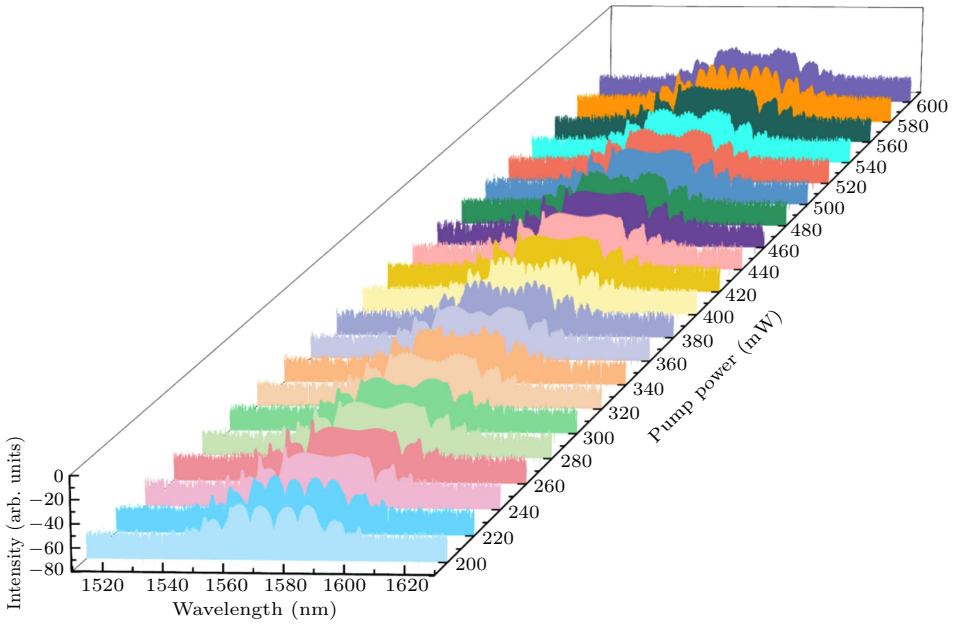


Fig. 3. Spectra of the L-band fiber laser at different pump powers.

To achieve a tunable mode-locked seed laser, stable self-starting mode locking was first obtained at a pump power of 200 mW by finely adjusting the intracavity polarization state. Subsequently, a tunable filter was inserted into the cavity to enable wavelength tuning. However, this insertion led to mode-locking instability due to spectral narrowing and increased intracavity loss. When the pump power was increased to 320 mW, stable mode locking was recovered. The pulse train was measured with a photodetector (DET08CFC, Thorlabs) connected to an oscilloscope (DS1204B, RIGOL), as shown in Fig. 4(a). The measured pulse interval was 64.1 ns, corresponding to a repetition rate of 15.6 MHz, which perfectly matched the calculated fundamental repetition rate derived from the cavity length. It can be seen that the laser operates in a fundamental mode-locked regime, producing a single pulse free from pulse splitting or higher-order harmonic mode locking.

To obtain the corresponding wavelength range in the cascaded SHG unit, the central wavelength of the output spectrum of the seed laser was set to 1588 nm by fine-tuning the filter angle, as shown in Fig. 4(b). Pulse durations were measured using an autocorrelator (FR-103XL, Femtochrome), as shown in Fig. 4(c). The recorded autocorrelation trace had a full width at half maximum of 124 ps. Assuming a sech^2 fitting function, this corresponds to an actual pulse width of 87 ps.

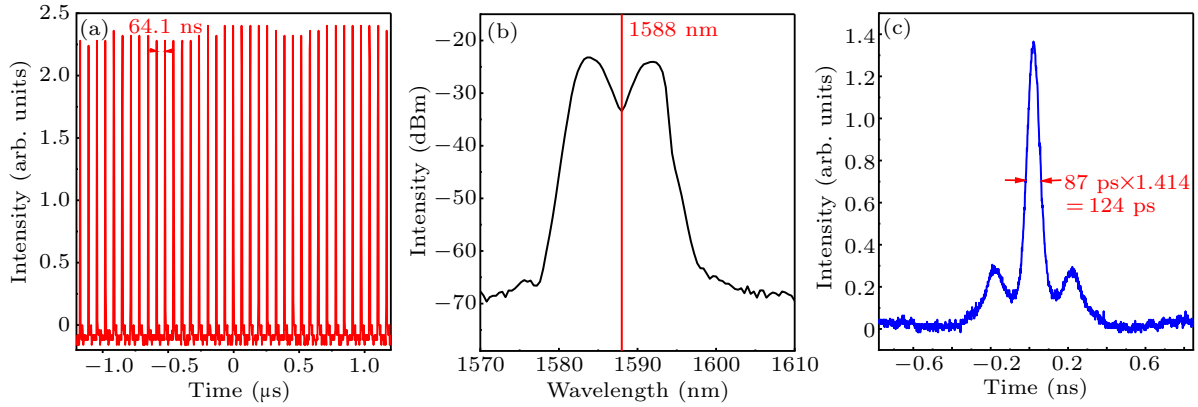


Fig. 4. (a) Output pulse train of the fiber laser. (b) Output spectrum of the fiber laser. (c) Intensity autocorrelation trace of the output pulse.

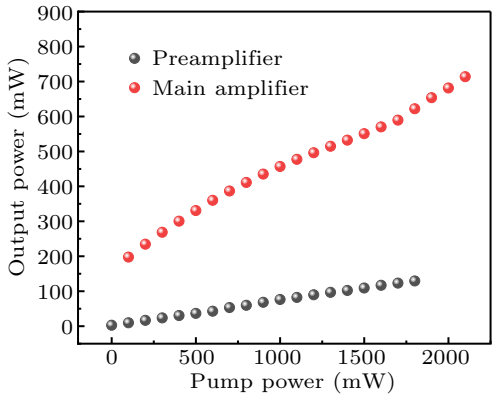


Fig. 5. Output powers of the preamplifier and main amplifier versus the pump power.

The optical power of the seed laser was amplified by a dual-stage EDFA, and the results are shown in Fig. 5. First, the seed laser was coupled into the preamplifier to enhance its pulse power while suppressing amplified spontaneous emission (ASE). It can be seen that the output power of the preamplifier shows a nearly linear relationship with its pump power, reaching a maximum of approximately 100 mW, indicating operation below the gain saturation regime. Subsequently, the amplified light was fed into the main amplifier. Owing to the use of a relatively long EDF, gain saturation was also absent in the main amplifier, whose output power likewise showed a linear dependence on the pump power. The maximum output power reached about 700 mW, which is sufficient for subsequent cascaded SHG.

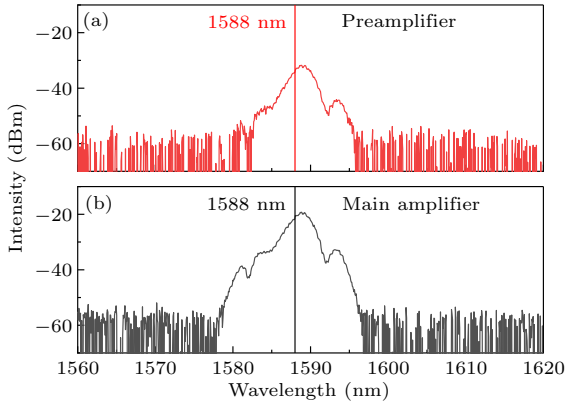


Fig. 6. (a) Output spectrum of the preamplifier. (b) Output spectrum of the main amplifier.

The output spectra of the preamplifier and main amplifier are shown in Figs. 6(a) and 6(b), respectively. It can be seen that the output spectrum of the preamplifier differs from the dual-peak spectrum of the seed laser shown in Fig. 4(b). This is because the gain of the EDF in the L-band decreases with increasing wavelength, causing the short-wavelength peak of the seed spectrum to experience higher gain and be amplified

into the dominant peak. Additionally, the relatively wide pulse width and normal dispersion of the EDF limit the peak power, thereby suppressing significant nonlinear spectral distortion in both the preamplifier and main amplifier. In the spectrum of the main amplifier, the Kelly sidebands near 1580 nm are clearly resolved, which is also attributable to the higher gain in that region.

We selected one of the central wavelengths (1588 nm) of the tunable L-band laser to analyze the cascaded SHG process. After optimizing the polarization of the 1588 nm pulses from the amplifier with an HWP, the pulses were first focused into the PPLN crystal using a lens with a focal length of 13.8 mm (D-ZK3, LBTEK), and the generated pulses were then collimated using another identical lens. By optimizing the temperature of the PPLN crystal, we obtained 794 nm pulses with a maximum conversion efficiency of 21%. These 794 nm pulses were then focused and collimated using two lenses with a focal length of 75 mm, respectively. Finally, by optimizing the angle of the BBO crystal, 397 nm UV pulses were generated with a maximum conversion efficiency of 2.4%. The 397 nm light was separated using a DM.

We measured the relationship between the input and output optical powers in the cascaded SHG process, as shown in Fig. 7. For the first SHG stage, the output power at 794 nm initially rose with an increasing slope as the input power at 1588 nm increased from 0 to 400 mW, beyond which the slope became constant. In contrast, for the second SHG stage, the output power at 397 nm increased almost linearly over the entire measured input power range of the 794 nm pulses. No saturation in conversion efficiency was observed in either stage.

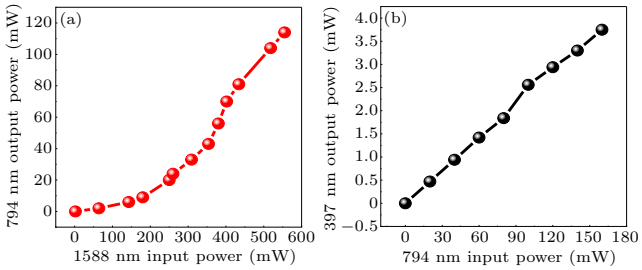


Fig. 7. (a) Second-harmonic output power from the PPLN crystal as a function of the input power of 1588 nm pulses. (b) Second-harmonic output power from the BBO crystal as a function of the input power of 794 nm pulses.

To enable the cascaded SHG unit to generate widely tunable near-infrared and UV light, we relied on the tuning of the PPLN poling period and the BBO phase-matching angle, taking advantage of the broad spectral bandwidth of the seed laser, while the intracavity filter in the seed laser provided initial wavelength selection. As shown in Fig. 8(a), with the tilt angle of the filter fixed, the second-harmonic wavelength was tuned from 778 nm to 804 nm by varying the PPLN poling period. This near-infrared output was then focused into the BBO crystal for SHG. By adjusting the BBO phase-matching angle, the fourth-harmonic output was tuned from 389 nm to 400 nm, as shown in Fig. 8(b). This tuning range covers the 397 nm transition required for calcium ion cooling and adjacent transitions for synergistic cooling. Owing to the upper detection limit of the UV spectrometer (PG2000PRO, IdeaOptics), the data in Fig. 8(b) are restricted to wavelengths up to 400 nm. Additionally, the signal-to-noise ratio in the UV region is reduced because fiber coupling for spectral detection leads to higher propagation losses at shorter wavelengths.

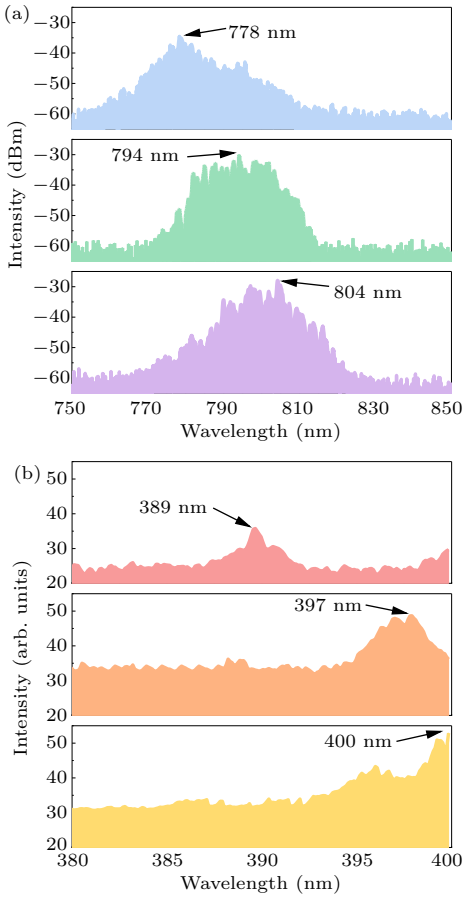


Fig. 8. (a) Wavelength tuning of the second harmonic. (b) Wavelength tuning of the fourth harmonic.

4. Conclusion

In this paper, we have described an all-PM, widely tunable L-band fiber laser based on an NALM. Through precise control of the tilt angle of the filter in this L-band laser, we achieved a tuning range of approximately 20 nm. This corresponded to a shift in the central wavelength from 1570 nm to 1590 nm. The L-band laser output was coupled to a dual-stage EDFA, and the amplified pulses were then directed into a cascaded SHG unit comprising PPLN and BBO crystals. This unit was designed to generate shorter-wavelength light through frequency doubling while preserving the tunability of the original source. For instance, starting from pulses of the L-band laser with a central wavelength of 1588 nm, we obtained tun-

able near-infrared pulses (778–804 nm) and UV pulses (389–400 nm). These results show that this laser system can function as a versatile and practical light source for advanced applications such as multi-ion quantum manipulation and ultrafast spectroscopy, benefiting from its broad tunability and robust all-PM fiber architecture.

Acknowledgement

This work was supported by the National Natural Science Foundation of China (Grant Nos. 62105368, 62275268, and 62375284).

References

[1] Srivastava A K, Radic S, Wolf C, Centanni J C, Sulhoff J W, Kantor K and Sun Y 2000 *IEEE Photonics Technol. Lett.* **12** 1570
[2] Morin F, Druon F, Hanna M and Georges P 2009 *Opt. Lett.* **34** 1991
[3] Bouma B E 1998 *J. Biomed. Opt.* **3** 76
[4] Shi L, Sordillo L A, Rodríguez-Contreras A and Alfano R 2016 *J. Biophotonics* **9** 38
[5] Jiang W, An W, Huang Z, Xu C, Shen Q, Pu C, Zhang S, Wu Q, Li L and Yu C 2024 *Talanta* **274** 126018
[6] Pietilainen A 1995 *Opt. Eng.* **34** 2637
[7] Guan H, Guo B, Huang G, Shu H, Huang X and Gao K 2007 *Opt. Commun.* **274** 182
[8] Dang L, Huang D, Su Z, Li Y and Li F 2025 *Opt. Laser Technol.* **181** 111944
[9] Song J, Liu Y and Zhang J 2019 *Appl. Opt.* **58** 7577
[10] Perez-Herrera R A, Roldan-Varona P, Sanchez-Gonzalez A, Rodriguez-Cobo L, Lopez-Higuera J M and Lopez-Amo M 2023 *J. Eur. Opt. Soc.-Rapid Publ.* **19** 2
[11] Jiang J, Huang Q, Ma Y, Liao D, Huang Z, Dai L, Liu Y, Mou C, Araimi M A and Rozhin A 2021 *Opt. Express* **29** 26332
[12] Li R, Chen C, Pan H, Chen Z, Zhang B, Zhao Z, Li Y and Li B 2024 *Opt. Quantum Electron.* **56** 1576
[13] Chen J, Zhu X, Sibbett W 1992 *J. Opt. Soc. Am. B* **9** 1876
[14] Franco P, Midrio M, Tozzato A, Romagnoli M and Fontana F 1994 *J. Opt. Soc. Am. B* **11** 1090
[15] Liu H H, Jiang Q, Song W, Yu Y, Li Z L and Pang F F 2019 *Chin. J. Lasers* **46** 0701007
[16] Mirza J, Ghafoor S, Atieh A, Kanwal B and Qureshi K K 2022 *J. Opt. Soc. Am. B* **39** 1118
[17] Li Q, Wang J Y, Ji X, Wang B, Chen X and Zheng Q 2023 *Infrared Laser Eng.* **52** 20230129
[18] Qureshi K K 2020 *Fiber Integr. Opt.* **39** 203
[19] Li R, Shi H, Tian H, Li Y, Liu B, Song Y and Hu M 2018 *Opt. Express* **26** 28302
[20] Tao J, Song P, Lv C, Hou L, Lu B and Bai J 2023 *Opt. Laser Technol.* **160** 109107
[21] Sun X, Zhu Y, Jin L, Yamashita S and Set S Y 2022 *Opt. Lett.* **47** 4913
[22] Ye G, Liu B, Dai M, Ma Y, Shirahata T, Yamashita S and Set S Y 2024 *Opt. Lett.* **49** 2433
[23] Tao J, Fang Y, Song Y, Song P, Hou L, Lu B, Lin Q and Bai J 2022 *Opt. Express* **30** 17465
[24] Jin X, Wang X, Wang X and Zhou P 2015 *Appl. Opt.* **54** 8260
[25] Qin F, Sun Y, Yang Y, Li X, Wang X, Lu J, Wang Y and Zhu G 2023 *Chin. Phys. B* **32** 054210
[26] Cui W W, Xing X W, Chen Y Q, Xiao Y J, Ye H and Liu W J 2023 *Chin. Phys. Lett.* **40** 024201
[27] Si Z Z, Dai C Q and Liu W 2024 *Chin. Phys. Lett.* **41** 020502
[28] Ren B, Li C, Wang T, Guo K and Zhou P 2023 *J. Light. Technol.* **41** 733
[29] Yang K, Feng L, Wei K, Liu C, Zhu H, Guo C, Yan P, Ruan S and Wang J 2022 *Opt. Lett.* **47** 4893
[30] Wang S, Li Y, Chen Y, Gao Y, Zhang Z and Wang A 2021 *Opt. Express* **29** 38199
[31] Fermann M E, Haberl F, Hofer M and Hochreiter H 1990 *Opt. Lett.* **15** 752
[32] Zhang H, Xia H, Zheng J, Li J, Zhang F, Fan M, Xiang X, Tian X, Huang Z, Zhang R, Li P, Peng Z, Hu D and Zhu Q 2024 *Opt. Express* **32** 25223
[33] Zhang Y, Zhang H, Gao K, Qiao W, Feng T, Zhao X and Liu Y 2023 *Photonics* **10** 665
[34] Gong Q, Zhang H, Deng D and Zu J 2020 *IEEE Photonics J.* **12** 1
[35] Graf F, Scelle R, Diekamp H, Budnicki A and Dekorsy T 2022 *Opt. Express* **30** 12555
[36] Mkrtchyan A A, Gladush Y G, Melkumov M A, Khegai A M, Sitnik K A, Lagoudakis P G, Nasibulin A G 2021 *J. Light. Technol.* **39** 5582
[37] Xu G, Wang S, Liang F, Lu D, Wu K, Zhang H, Yu H, Yu P and Wang Z 2025 *Appl. Phys. B* **131** 28
[38] Wu W D, Ren T Q, Zhou J, Du S T and Liu X 2012 *Chin. Opt. Lett.* **10** 050604
[39] Beyer M, Roth J C, Edwards E and DeMille D 2021 *Opt. Express* **29** 20370
[40] Si G, Song W, Hou Y, Zhao H, Zhang Q and Wang P 2024 *Opt. Commun.* **561** 130451
[41] Zhao H, Li K Y, Dai S B, Tu Z H, Yang Q G, Zhu S Q, Yin H, Li Z and Chen Z Q 2021 *Opt. Lett.* **46** 3207
[42] Huang T C, Chen H X, Li H F, Gu P F and Shen Y B 2003 *Acta Photonica Sin.* **32** 1438 ISSN: 1004-4213
[43] Yu K X, Zhu X Y and Wu C 2021 *Opto-Electron Eng.* **48** 210173